DSP-enabled reconfigurable and transparent spectral converters for converging optical and mobile fronthaul/backhaul networks

Mao, M. Z.; Giddings, Roger; Cao, B. Y.; Xu, Y. T. ; Wang, M.; Tang, Jianming

Optics Express

Cyswllt i'r cyhoeddiad / Link to publication

09. Oct. 2020

DSP-enabled reconfigurable and transparent spectral converters for converging optical and mobile fronthaul/backhaul networks

M. Z. Mao,[1] R. P. Giddings,[2] B. Y. Cao,[1] Y. T. Xu,[1] M. Wang,[1] and J. M. Tang[2,*]

[1]*Key Laboratory of Specialty Fiber Optics and Optical Access Networks, Shanghai University, Shanghai 200072, China*
[2]*School of Electronic Engineering, Bangor University, Bangor, LL57 1UT, UK*
*j.tang@bangor.ac.uk

Abstract: Dynamically reconfigurable and transparent signal spectral conversion is expected to play a vital role in seamlessly integrating traditional metropolitan optical networks and mobile fronthaul/backhaul networks. In this paper, a simple digital signal processing (DSP)-enabled spectral converter is proposed and extensively investigated, for the first time, which just utilizes a single standard dual-parallel Mach-Zehnder modulator (DP-MZM) driven by SDN-controllable RF signals and DC bias currents. As an important thrust of the paper, optimum operating conditions of the proposed converter are analytically identified, statistically examined and experimentally verified. Optimum operating condition-supported spectral converter performances in IMDD-based network nodes are explored both theoretically and experimentally in terms of frequency detuning range-dependent conversion efficiency, spectral conversion-induced OSNR/power penalty and transparency to input signal characteristics. The proposed spectral converter has unique advantages including low configuration complexity, strict transparency, SDN-controllable performance reconfigurability and flexibility, as well as negligible spectral conversion-induced latency.

References and links

1. J. E. Mitchell, "Integrated wireless backhaul over optical access networks," J. Lightwave Technol. **32**(20), 3373–3382 (2014).
2. P. Chanclou, A. Cui, F. Geilhardt, J. Nakamura, and D. Nesset, "Network operator requirements for the next generation of optical access networks," IEEE Netw. **26**(2), 8–14 (2012).
3. Y. Okumura and J. Terada, "Optical network technologies and architectures for backhaul/fronthaul of future radio access supporting big mobile data," in *Optical Fiber Communication Conference* (Optical Society of America, 2014), Paper Tu3F.1.
4. M. Channegowda, R. Nejabati, and D. Simeonidou, "Software-defined optical networks technology and infrastructure: enabling software-defined optical network operations [Invited]," J. Opt. Netw. **5**(10), A274–A282 (2013).
5. A. E. Willner, S. Khaleghi, M. R. Chitgarha, and O. F. Yilmaz, "All-optical signal processing," J. Lightwave Technol. **32**(4), 660–680 (2014).
6. S. J. B. Yoo, "Wavelength conversion technologies for WDM network applications," J. Lightwave Technol. **14**(6), 955–966 (1996).
7. A. Nguyen, C. Porzi, G. Serafino, F. Fresi, G. Contestabile, and A. Bogoni, "All-optical gated wavelength converter-eraser using a single SOA-MZI," IEEE Photonics Technol. Lett. **23**(21), 1621–1623 (2011).
8. G. Contestabile, Y. Yoshida, A. Maruta, and K. Kitayama, "Ultra-broad band, low power, highly efficient coherent wavelength conversion in quantum dot SOA," Opt. Express **20**(25), 27902–27907 (2012).
9. E. Temprana, V. Ataie, A. Peric, N. Alic, and S. Radic, "Wavelength conversion of QPSK signals in single-pump FOPA with 20 dB conversion efficiency," in Optical Fiber Communication Conference, (Optical Society of America, 2014), Paper Th1H.2.
10. H. Murai, Y. Kanda, M. Kagawa, and S. Arahira, "Regenerative SPM-based wavelength conversion and field demonstration of 160-Gb/s all-optical 3R operation," J. Lightwave Technol. **28**(6), 910–921 (2009).
11. D. Zhu and J. Yao, "Dual-chirp microwave waveform generation using a dual-parallel Mach–Zehnder modulator," IEEE Photonics Technol. Lett. **27**(13), 1410–1413 (2015).

12. Z. Cao, J. Yu, F. Li, L. Chen, Q. Shu, Q. Tang, and L. Chen, "Energy efficient and transparent platform for optical wireless networks based on reverse modulation," IEEE J. Sel. Areas Comm. **31**(12), 804–814 (2013).
13. W. Jin, X. Duan, Y. Dong, B. Cao, R. P. Giddings, C. F. Zhang, K. Qiu, and J. M. Tang, "DSP-enabled flexible ROADMs without optical filters and O-E-O conversions," J. Lightwave Technol. **33**(19), 4124–4131 (2015).
14. W. Jin, C. F. Zhang, X. Duan, M. R. Kadhum, Y. X. Dong, R. P. Giddings, N. Jiang, K. Qiu, and J. M. Tang, "Improved performance robustness of DSP-enabled flexible ROADMs free from optical filters and O-E-O conversions," J. Opt. Commun. Netw. **8**(8), 521–529 (2016).
15. X. Duan, M. L. Deng, W. Jin, R. P. Giddings, S. Mansoor, and J. M. Tang, "Experimental demonstration of DSP-enabled drop operations of flexible ROADMs excluding optical filters and O-E-O conversions," in Optical Fiber Communication Conference, (Optical Society of America, 2016), Paper M3E.4.
16. M. Abramowitz and I. A. Stegun, *Handbook of Mathematical Functions* (Dover Publications Inc. 1968).

1. Introduction

To satisfy the ever-increasing data traffic growth associated with a considerably diversified range of unprecedented emerging Internet applications and services, recent years have seen fast growing research interest in seamlessly integrating traditional optical access networks, metropolitan optical networks and mobile fronthaul/backhaul networks [1–3]. In particular, for achieving the highly desired convergence of existing metropolitan optical networks and future mobile backhaul networks, advanced networking devices of excellent cost-effectiveness, compact footprint and low power consumption are required in corresponding network nodes. Those networking devices enable the converged networks to not only adapt to the highly dynamic traffic with arbitrary bandwidth granularity, but also simultaneously accommodate various major network design features including, for example, transmission capacity versus reach performance, signal modulation format, signal modulation/detection scheme, wavelength division multiplexing (WDM) grid, as well as multiple access technique. In addition, it is also vital for those advanced networking devices to be equipped with a wide diversity of software-defined networking (SDN) functionalities to provide dynamically reconfigurable connections and services at reduced latency [4].

As one of the most important networking devices embedded in a representative converged network node, a simple and low-cost spectral converter is vital for performing SDN-controllable reconfigurable and transparent signal spectral conversion at frequency detuning ranges of up to a few hundred GHz. The implementation of such a converter ensures the delivery of the abovementioned salient features of the converged networks, and also allows the converged networks to have greatly enhanced reconfigurability, flexibility and elasticity, as well as effectively minimized latency and traffic blocking probability.

Technically speaking, depending upon the physical mechanisms underpinning the spectral conversion operation, previously reported spectral converters can be generally classified into three main categories [5] namely, optical-electrical-optical (O-E-O)-based optoelectronic converters, optical gating-based converters and wave-mixing–based converters. For practical implementation in the network scenarios of interest of the present paper, all these existing converters, however, suffer from a number of serious impediments, which include, for example, extremely low power consumption efficiency, high configuration complexity, considerably large capital expenditure (CapEx) and operational expenditure (OpEx) [6], as well as no SDN controllability in the physical layer.

In addition to the aforementioned common implementation-associated challenges, each of these converter categories also has its own technical difficulties directly related to its physical operation mechanism. Firstly, for the optoelectronic converter category, its O-E-O operation gives rise to limited performance transparency, and its reconfigurability and flexibility are also very restricted as a specific converter is often designed and optimized only for a well-defined system/network architecture subject to pre-determined traffic conditions. Secondly, for the optical gating-based converter category, the constrained performance transparency, reconfigurability and flexibility still remain because of the employment of the input data to gate the new wavelength [7]. Furthermore, such converter's typical long transition lifetime not only further constrains its maximum achievable conversion performance, but also causes

various distortions to converted signals [6]. Thirdly, to generate a new spectrally inversed optical signal of a different wavelength, the wave-mixing converter category employs nonlinear medium-based optical grating induced by simultaneously injected pump and probe optical signals [8]. As a direct result, compared with other two converter categories, such a converter category offers strict transparency and improved reconfigurability, but confronts the highest degree of converter configuration complexity. In addition, the converter performance is also heavily dependent upon pump power. The achievable maximum power of the optical pump propagating in the nonlinear medium is, however, physically constrained by stimulated Brillouin scattering (SBS) [9], and the corresponding pump optical source is also very bulky and expensive.

From the above descriptions, it is easy to understand that all of these three converter categories also have the following three drawbacks: i) requirements of extra light sources; ii) restricted operation reconfigurability and flexibility, as their spectral operation characteristics are difficult to vary over a wide range according to dynamic traffic and network status; and iii) inevitable distortions of converted signal waveforms [10] (3R regeneration in the optoelectronic category is not preferred because of O-E-O-induced large latency).

Since all the existing spectral converters are not suitable for the cost-sensitive application scenarios considered here, the thrust of this paper is, therefore, to propose and extensively investigate, for the first time, a simple digital signal processing (DSP)-enabled, reconfigurable and transparent signal spectral converter. The proposed signal spectral converter just utilizes a single standard dual-parallel Mach-Zehnder modulator (DP-MZM) driven by SDN-controllable RF signals and DC bias currents. The proposed converter makes full use of a well-known phenomenon, i.e. a RF signal-driven DP-MZM subject to an input optical signal produces a set of driving signal frequency-spaced optical components governed by the Bessel function of first kind [11]. A significantly innovative aspect of this paper is, for the first time, to numerically identify, statistically explore and experimentally verify the optimum DP-MZM operating conditions, under which the power of a converted optical component at the targeted frequency detuning range is maximized, whist the powers of all other unwanted parasitic optical components are minimized simultaneously. In addition, optimum operating condition-supported spectral converter performances in intensity-modulation and direct-detection (IMDD)-based network nodes are also extensively explored both theoretically and experimentally in terms of frequency detuning range-dependent conversion efficiency, signal spectral conversion-induced optical signal-to-noise ratio (OSNR)/power penalty, as well as spectral conversion performance transparency to input signal characteristics. Moreover, discussions are also made of opportunities for further simplifying the proposed converter architecture.

In comparison with the existing three types of spectral converters, the unique advantages associated with the proposed converter are summarized as followings:

- Extremely low converter configuration complexity. The proposed converter just consists a single standard DP-MZM only, and does not require any extra optical light sources. As such, this can considerably lower the converter's CapEx and OpEx.

- Strict operation transparency. As detailed in Section 4 and Section 5, the spectral conversion performance is independent of the input optical signal characteristics including signal bit rates, signal modulation formats, optical signal powers, as well as signal modulation schemes.

- SDN-controllable reconfigurability, flexibility, scalability and elasticity with network control further extended to the physical layer. Based on SDN-associated network intelligence, use can be made of simple embedded simple DSP algorithms to dynamically alter the converter's operation properties in terms of spectral conversion efficiency, frequency detuning range, allowable signal spectral bandwidth,

conversion-induced OSNR/power penalty, as well as trade-offs between these features mentioned above.

- Negligible conversion-induced latency. The spectral conversion is performed in the optical domain and the converted signal waveform is almost distortionless, suggesting that relatively low DSP complexity is sufficient for DSP-based system impairment compensation and signal recovery. Apart from that, DSP used to control the converter operating conditions is also simple. As a direct result, negligible spectral conversion-induced latency is expected for the proposed converter.
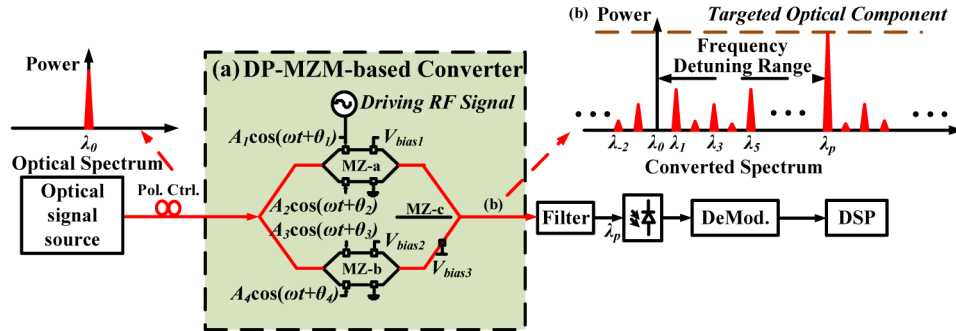

Fig. 1. (a) Schematic illustration of the proposed spectral converter utilizing a single standard DP-MZM. (b) Representative converted optical components and frequency detuning range definition.

2. Operating principle and optimum operating condition identification

2.1 Operating principle

The schematic diagram of the proposed DSP-enabled spectral converter is illustrated in the green-shaded area of Fig. 1(a). The converter just utilizes a single standard DP-MZM, which consists of two parallel dual-drive Mach-Zehnder modulators (DD-MZMs), MZ-a and MZ-b, as well as a phase modulator, MZ-c [12]. As shown in Fig. 1(a), when an optical signal encoded using an arbitrary signal modulation format is injected into the DP-MZM subject to four driving RF signals and three DC bias currents, the DP-MZM splits the input optical signal into two separate paths, MZ-a and MZ-b, each of which converts the split optical signal into a set of driving RF signal frequency-spaced optical components governed by the Bessel function of first kind. Whilst MZ-c controls the phase difference between these two optical component sets, and the combination of these two sets gives rise to a final set of converted optical components, as illustrated in Fig. 1(b). Detailed mathematical descriptions of the abovementioned processes can be found in Subsection 2.2.

Within the final converted optical component set, each individual optical component carries the same information conveyed by the input optical signal. If the *p-th* optical component is selected as the converted optical component, its spectral conversion efficiency can be defined as the optical power ratio between the *p-th* converted optical component and the input optical signal. Whilst the corresponding frequency detuning range can be defined as the difference between the central frequencies of the *p-th* converted optical component and the input optical signal, as indicated in Fig. 1(b). It is easy to understand that, via appropriately adjusting these four driving RF signals and three DC bias currents, the operating conditions of the proposed spectral converter can be optimized dynamically to simultaneously achieve the following three highly desired performance features, including: i) a maximized conversion efficiency of the *p-th* converted optical component; ii) an enhanced frequency difference between two adjacent converted optical components for a specific driving RF signal frequency, and iii) the minimized count of unwanted parasitic optical

components. Such optimum operating conditions are identified analytically in Subsection 2.3, subsequently explored statistically in Section 3, and experimentally verified in Section 5.

It should also be noted that, in practice, each individual signal spectral converter embeds a dedicated DSP controller, which is responsible for dynamically optimizing the converter operating conditions, via periodically communicating with both DSP controllers embedded in other relevant converters/transceivers and the centralized SDN controller. The centralized SDN controller also performs centralized network resource abstraction and network infrastructure virtualization. In addition, the centralized SDN controller also exchanges information with each individual converter-embedded DSP controller utilizing extended OpenFlow. Based on such information exchange, both the four driving RF signals and three DC bias currents can be adjusted dynamically to convert an input signal into a targeted spectral region according to traffic and transmission link characteristics. Therefore, on-line SDN reconfigurable and flexible signal spectral conversion is feasible for the application scenarios considered here.
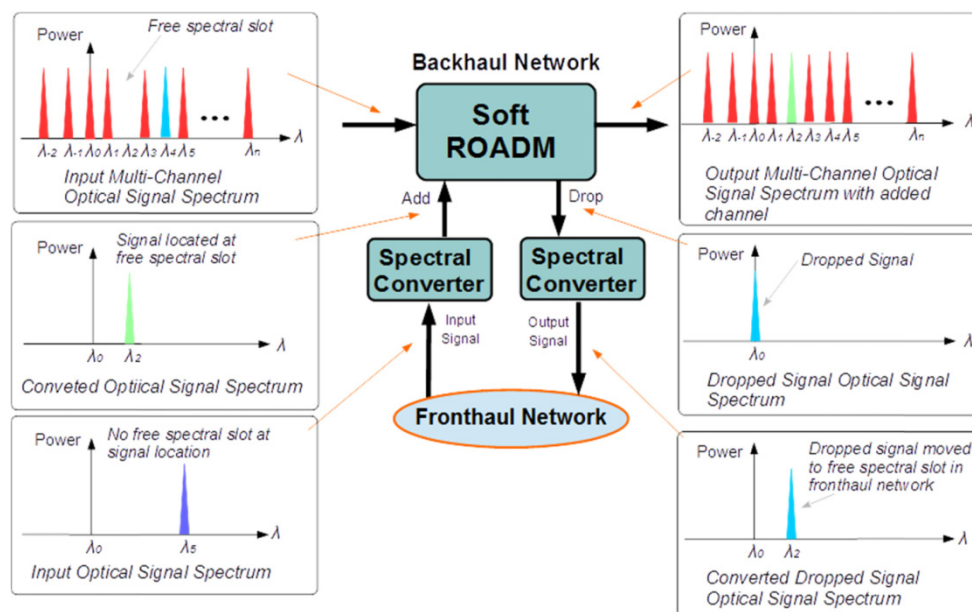

Fig. 2. An illustration of utilizing spectral converters with a soft-ROADM to dynamically integrate mobile fronthaul and backhaul networks.

Here it is worth mentioning the fact that, as discussed in Section 4 and Section 5 of the present paper, the frequency detuning range of the proposed spectral converter is typically a few hundred GHz, which is considerably smaller compared to those associated with existing optical converters designed for conventional WDM optical networks. As such, the proposed spectral converters are targeted for application scenarios where the aforementioned frequency detuning range without involving complicated O-E-O conversion is sufficient. To dynamically integrate mobile fronthaul and backhaul networks, and also to create a programmable environment capable of addressing elastic 5G slicing and SDN paradigm, an example of how the proposed spectral converter can be utilized is illustrated in Fig. 2, where a DSP-enabled reconfigurable optical add/drop multiplexer (ROADM) [13–15] is also shown. Considering an upstream transmission link from the fronthaul to the backhaul, an optical signal at a specific RF spectral region needs to be added to a backhaul optical signal conveying multiple RF signal bands with a channel spacing of up to 40MHz. As shown in Fig. 2, when the backhaul spectral region required by the fronthaul signal is occupied, to reduce the traffic blocking probability, the spectral converter has to be employed to shift the

fronthaul signal spectrum to a free region of the backhaul spectrum, before performing the add operation using the ROADM. On the other hand, for a downstream transmission link from the backhaul to the fronthaul, the ROADM-dropped signal occupies the baseband only, thus another spectral converter is needed to shift the dropped baseband signal to a RF spectral region required by a specific remote radio head (RRH). From the above-discussed example, it is also easy to understand that, in addition to the integrated network with highly desired networking features, the proposed spectral converter also allows the employment of cheap optical modulators in RRHs.

2.2 Mathematical descriptions of converted optical components

Based on [11] and Fig. 1(a), assuming that the DP-MZM has a switching voltage of $V\pi$, and MZ-a (MZ-b) has a DC bias voltage of V_{bias1} (V_{bias2}) for one DC electrode with the other DC electrode being grounded, for an input optical signal, $A(t){\cdot}\exp(j\omega_c t + j\theta_c)$, the output optical signals from MZ-a and MZ-b, $E_{out\text{-}up}$ and $E_{out\text{-}down}$, can thus be written as:

$$\begin{cases} E_{out\_up}(t) = \frac{A(t)e^{j(\omega_c t + \theta_c)}\sqrt{t_{ff}}}{4}\left\{ \begin{array}{l} e^{j\left(\Delta\varphi_{up}+\beta_1\cos(\omega_{rf}t+\theta_1)\right)} \\ +e^{j\left(\beta_2\cos(\omega_{rf}t+\theta_2)\right)} \end{array} \right\} \\ E_{out\_down}(t) = \frac{A(t)e^{j(\omega_c t + \theta_c)}\sqrt{t_{ff}}}{4}\left\{ \begin{array}{l} e^{j\left(\Delta\varphi_{down}+\beta_3\cos(\omega_{rf}t+\theta_3)\right)} \\ +e^{j\left(\beta_4\cos(\omega_{rf}t+\theta_4)\right)} \end{array} \right\} \end{cases} \quad (1)$$

where $A(t)$, ω_c, and θ_c represent the amplitude, the central angular frequency and the phase of the input optical signal, respectively. $\Delta\varphi_{up} = V_{bias1}{\bullet}\pi/V_\pi$ and $\Delta\varphi_{down} = V_{bias2}{\bullet}\pi/V_\pi$ are the normalized bias phases. $\beta_i = A_i{\bullet}\pi/V_\pi$ ($i = 1, 2, 3, 4$) is the modulation index with A_i, ω_{rf} and θ_i being the driving RF signal amplitude, the angular RF frequency and the phase, respectively. t_{ff} is the DP-MZM insertion loss. By applying the Jacobi-Anger expansion to Eq. (1), the converted optical signal emerging from the DP-MZM is given by:

$$E_{out}(t) = E_{out\_up}(t) + e^{j\phi}E_{out\_down}(t)$$

$$= \frac{A(t)e^{j(\omega_c t + \theta_c)}\sqrt{t_{ff}}}{4}\left\{ \begin{array}{l} +\sum_{k=-\infty}^{\infty}J_k(\beta_1)e^{j\left[\Delta\varphi_{up}+\frac{k\pi}{2}+k(\omega_{rf}t+\theta_1)\right]} + \sum_{k=-\infty}^{\infty}J_k(\beta_2)e^{j\left[\frac{k\pi}{2}+k(\omega_{rf}t+\theta_2)\right]} \\ +e^{j\phi}\sum_{k=\infty}^{\infty}J_k(\beta_3)e^{j\left[\Delta\varphi_{down}+\frac{k\pi}{2}+k(\omega_{rf}t+\theta_3)\right]} + e^{j\phi}\sum_{k=\infty}^{\infty}J_k(\beta_4)e^{j\left[\frac{k\pi}{2}+k(\omega_{rf}t+\theta_4)\right]} \end{array} \right\}$$

$$(2)$$

where k is the order of the Bessel function of first kind. ϕ represents the phase difference associated with MZ-c.

When the *p-th* optical component is selected as the converted optical component, by making use of Eq. (2), the expression of the *p-th* converted optical component is:

$$E_{out}\left(\omega_c t + p(\omega_{rf}t)\right) = \frac{A(t)\sqrt{t_{ff}}}{4}K_p e^{j\left(\omega_c t + \theta_c + p\omega_{rf}t + \frac{p\pi}{2}\right)} \quad (3)$$

where K_p is defined by:

$$K_p = J_p(\beta_1)e^{j(\Delta\varphi_{up}+p\theta_1)} + J_p(\beta_2)e^{j(p\theta_2)} + J_p(\beta_3)e^{j(\Delta\varphi_{down}+p\theta_3+\phi)} + J_p(\beta_4)e^{j(p\theta_4+\phi)} \quad (4)$$

Based on Eq. (3), the spectral conversion efficiency of the *p-th* converted optical component is defined by:

$$\eta_p = \frac{t_{ff}\left|K_p\right|^2}{16} \tag{5}$$

where $|K_p|^2$ has a form given below

$$\left|K_p\right|^2 = \begin{cases} J_p^2(\beta_1) + J_p^2(\beta_2) + J_p^2(\beta_3) + J_p^2(\beta_4) \\ +2J_p(\beta_1)J_p(\beta_2)\cos\left(p\theta_1 - p\theta_2 + \Delta\varphi_{up}\right) \\ +2J_p(\beta_1)J_p(\beta_3)\cos\left(p\theta_1 - p\theta_3 + \Delta\varphi_{up} - \Delta\varphi_{down} - \phi\right) \\ +2J_p(\beta_1)J_p(\beta_4)\cos\left(p\theta_1 - p\theta_4 + \Delta\varphi_{up} - \phi\right) \\ +2J_p(\beta_2)J_p(\beta_3)\cos\left(p\theta_2 - p\theta_3 - \Delta\varphi_{down} - \phi\right) \\ +2J_p(\beta_2)J_p(\beta_4)\cos\left(p\theta_2 - p\theta_4 - \phi\right) \\ +2J_p(\beta_3)J_p(\beta_4)\cos\left(p\theta_3 - p\theta_4 + \Delta\varphi_{down}\right) \end{cases} \tag{6}$$

2.3 Identification of optimum operating conditions

For the *p-th* converted optical component, it is clear from Eq. (5) that the maximum spectral conversion efficiency is achievable only when $|K_p|^2$ reaches its maximum value. To maximize $|K_p|^2$, it is easy to understand from Eq. (6) that the following two requirements have to be met simultaneously: a) each of the four terms occurring in the first line of Eq. (6) takes its highest value, and b) each of the cosine functions in Eq. (6) is equal to 1. Considering the well-known *p-th* Bessel function expression, from Eq. (6) the following converter operating conditions can thus be obtained:

$$\begin{cases} p\theta_1 - p\theta_2 + \Delta\varphi_{up} = 2m\pi \\ p\theta_1 - p\theta_4 + \Delta\varphi_{up} - \phi = 2m\pi \\ p\theta_2 - p\theta_3 - \Delta\varphi_{down} - \phi = 2m\pi \\ p\theta_3 - p\theta_4 + \Delta\varphi_{down} = 2m\pi \\ \beta_{p\_opt} = \beta_1 = \beta_2 = \beta_3 = \beta_4 \end{cases} \tag{7}$$

where $m = 0, \pm 1, \pm 2, \pm 3,\ldots$, and β_{p_opt} is the modulation index corresponding to the highest *p-th* Bessel function value. Equation (7) governs the converter operating conditions, under which the highest spectral conversion efficiency is obtainable for the *p-th* converted optical component.

Apart from the highest spectral conversion efficiency, the number of unwanted parasitic optical components occurring at the output of the converter should also be minimized. For a given driving RF signal frequency, this cannot only enhance the frequency detuning range but also considerably reduce possible cross-talks induced by the parasitic optical components. As such, further analytical treatments should also be undertaken to the converter operating conditions presented in Eq. (7). The analytical procedure can be divided into two separate stages: Stage I- the elimination of the zero-order optical component, and Stage II- the minimization of the number of unwanted parasitic optical components.

In Stage I, by introducing Eq. (7) into Eq. (4), K_0 corresponding to the zero-order converted optical component has a form expressed below:

$$K_0 = 2J_o\left(\beta_{p\_opt}\right)\left[\cos\frac{\Delta\varphi_{up}}{2}e^{j\frac{\Delta\varphi_{up}}{2}} + e^{j\phi}\cos\frac{\Delta\varphi_{down}}{2}e^{j\frac{\Delta\varphi_{down}}{2}}\right] \tag{8}$$

Equation (8) indicates that, to eliminate the zero-order optical component, two cases can be considered: Case I, $E_{out\text{-}up}$ and $E_{out\text{-}down}$ are offset completely, and Case II, the zero-order optical component does not occur in either $E_{out\text{-}up}$ or $E_{out\text{-}down}$. The corresponding converter operating conditions capable of eliminating the zero-order optical component can thus be obtained as:

$$\begin{cases} \Delta\varphi_{up}=\Delta\varphi_{down} \quad \& \quad \phi=(2m-1)\pi, \quad for \ case \ I \\ \Delta\varphi_{up}=\Delta\varphi_{down}=\pi+2m\pi, \quad for \ case \ II \end{cases} \tag{9}$$

On the other hand, in Stage II, to further eliminate the k-th parasitic optical component, by introducing Eqs. (7) and (9) into Eq. (4), K_k corresponding to the k-th parasitic optical component can be written as:

$$K_k = J_k\left(\beta_{p\_opt}\right)\left[\begin{array}{l} 2\cos\left(k\dfrac{\theta_1-\theta_3}{2}-\dfrac{\phi}{2}\right)e^{j\left(\frac{\Delta\varphi_{up}+\Delta\varphi_{down}+k\theta_1+k\theta_3+\phi}{2}\right)} \\ +2\cos\left(k\dfrac{\theta_2-\theta_4}{2}-\dfrac{\phi}{2}\right)e^{j\left(\frac{k\theta_2+k\theta_4+\phi}{2}\right)} \end{array}\right] \tag{10}$$

It can be seen in Eq. (10) that, depending upon the even- ($k = \pm 2n$) and odd- ($k = \pm (2n-1)$) order of k, all the parasitic optical components can be classified into two groups: an even group and an odd group. The operating conditions capable of removing all parasitic optical components in the even group can be easily obtained by solving Eq. (10) at $K_{k|k = \pm 2n} = 0$. The resulting operating conditions are thus given by:

$$\begin{cases} \phi=(2m-1)\pi \\ \theta_1-\theta_3=(2m-1)\pi \\ \theta_2-\theta_4=(2m-1)\pi \end{cases} \tag{11}$$

Following the identical procedure adopted in obtaining Eq. (10), the parasitic optical components in the odd group can be expressed as:

$$E_{out}(t) = E_{out\_up}(t)+e^{j\phi}E_{out\_down}(t)$$
$$= \underbrace{A(t)\sqrt{t_{ff}}J_{p\_max}\left(\beta_{p\_opt}\right)e^{j\left[\omega_c t+p\omega_{rf}t+\theta_c+\Psi_p\right]}}_{Converted\ optical\ component}$$
$$+A(t)\sqrt{t_{ff}}\sum_{k=-\infty,k\neq p}^{\infty}J_k\left(\beta_{p\_opt}\right)\times\left[\cos\left(\frac{(p-k)}{2}\frac{(\theta_1-\theta_2+\theta_3-\theta_4)}{2}\right)e^{j\left[\omega_c t+k\omega_{rf}t+\theta_c+\Psi_k\right]}\right] \tag{12}$$

where Ψ_p is the p-th converted optical component phase having a form given by:

$$\Psi_p = \frac{\Delta\varphi_{up}+\Delta\varphi_{down}+2p\pi+p(\theta_1+\theta_2+\theta_3+\theta_4)}{4} \tag{13}$$

It can be easily seen in Eq. (12) that half of the odd parasitic optical components can be removed when the following operating condition is satisfied:

$$\frac{(\theta_1-\theta_2+\theta_3-\theta_4)}{2} = \left(\frac{\pi}{2}+m\pi\right) \tag{14}$$

Based on the above analysis, the final output of the converted optical signal field at the output of the DP-MZM can be written as:

$$
\begin{aligned}
E_{out} &= E_{out\_up} + e^{j\phi} E_{out\_down} \\
&= \underbrace{A(t)\sqrt{t_{ff}} J_{p\_max}\left(\beta_{p\_opt}\right) e^{j\left(\omega_c t + p\omega_{rf} t + \theta_c + \Psi_p\right)}}_{Converted\ optical\ component}
\end{aligned}
$$

$$
+ \underbrace{A(t)\sqrt{t_{ff}} J_p\left(\beta_{p\_opt}\right)
\begin{bmatrix}
+... \\
+J_{p-8}\left(\beta_{p\_opt}\right) e^{j\left(\omega_c t + (p-8)\omega_{rf} t + \theta_c + \Psi_{(p-8)}\right)} \\
-J_{p-4}\left(\beta_{p\_opt}\right) e^{j\left(\omega_c t + (p-4)\omega_{rf} t + \theta_c + \Psi_{(p-4)}\right)} \\
-J_{p+4}\left(\beta_{p\_opt}\right) e^{j\left(\omega_c t + (p+4)\omega_{rf} t + \theta_c + \Psi_{(p+4)}\right)} \\
+J_{p+8}\left(\beta_{p\_opt}\right) e^{j\left(\omega_c t + (p+8)\omega_{rf} t + \theta_c + \Psi_{(p+8)}\right)} \\
+...
\end{bmatrix}}_{Parasitic\ optical\ components}
\tag{15}
$$

Based on Eqs. (5) and (15), the highest conversion efficiency of the *p-th* converted optical component can be expressed as:

$$
\eta_p = J^2_{p\_max}\left(\beta_{p\_opt}\right) t_{ff}
\tag{16}
$$

Reorganizing the operating conditions presented in Eqs. (7), (9), (11) and (14), the final optimum operating conditions of the proposed converter are:

$$
\begin{cases}
\phi = \pi + 2m\pi \\
\Delta\theta = \Delta\theta_{12} = \Delta\theta_{23} = \Delta\theta_{34} = \Delta\theta_{41} = \dfrac{\pi}{2} + m\pi \\
\Delta\varphi_{up} = \Delta\varphi_{down} = -p\Delta\theta \\
\beta_{p\_opt} = \beta_1 = \beta_2 = \beta_3 = \beta_4
\end{cases}
\tag{17}
$$

with $\Delta\theta_{12} = \theta_1-\theta_2$, $\Delta\theta_{23} = \theta_2-\theta_3$, $\Delta\theta_{34} = \theta_3-\theta_4$, $\Delta\theta_{41} = \theta_4-\theta_1$. Equation (17) is the identified optimum operating conditions, under which the DP-MZM-based spectral converter simultaneously offers the highest spectral conversion efficiency and the minimized number of unwanted parasitic optical components. As all the even-order optical components and half of the odd-order optical components are eliminated, the optimum operation conditions can thus reduce 75% of the parasitic optical components. In addition, it should also be pointed out that Eq. (17) enables not only the lowest bit error rate (BER) performance of the *p-th* converted optical component but also a 4 × enhanced frequency difference between two adjacent converted optical components, as discussed in Sections 3, 4 and 5.

3. Statistical verifications of identified optimum operating conditions

Having analytically identified the optimum operating conditions in Section 2, statistical verifications of the identified optimum operating conditions are, therefore, undertaken in Section 3 through numerically exploring the optimum operating conditions-supported major converter performances in terms of the maximization of the spectral conversion efficiency, and the reduction in parasitic optical component count. In addition, in this Section, the optimum operation condition-induced minimization of BERs of various converted optical components is also numerically explored, which, however, cannot be analytically addressed

using the approach presented in Section 2. To achieve these technical tasks, extensive comparisons of the proposed converter performances are made between the cases where the optimum operating conditions are adopted and the cases where converter operating condition parameters are randomly selected within their entire dynamic ranges.

In numerically simulating the optimum operating condition cases, to ensure that the highest Bessel function value is chosen for a specific converted optical component, the modulation index β_{p_opt} are fixed at 1.84, 4.20, 6.42, 8.58 and 10.71 when the 1-, 3-, 5-, 7- and 9-*th* converted optical components are targeted [16], respectively. In addition, the phase differences between the four driving RF signals are fixed at $\Delta\theta = -\pi/2$ ($\theta_1 = 0$, $\theta_2 = \pi/2$, $\theta_3 = \pi$, $\theta_4 = 3\pi/2$), and the corresponding three normalized bias phases, $\Delta\varphi_{up}$, $\Delta\varphi_{down}$ and ϕ, are taken to be $p\pi/2$, $p\pi/2$ and π, respectively.

On the other hand, for statistically exploring the performances of the converters subject to randomly selected operating condition parameters, all these seven phase parameters, namely θ_1, θ_2, θ_3, θ_4, $\Delta\varphi_{up}$, $\Delta\varphi_{down}$ and ϕ, are treated as independent variables. In simulating each individual scenario such as spectral conversion efficiency for a specific converted optical component, 1600 different numerical simulations are performed, in each of these individual simulations, these seven phase parameter values are randomly selected within their entire dynamic ranges from 0 to 2π at a uniform distribution probability. In addition, the modulation index parameters identical to those corresponding to the optimum operating condition cases are still adopted to effectively shorten the computation execution time. More importantly, for a given set of randomly selected phase parameters, such a choice of optimum modulation index parameters can always enhance the converter performance, as a direct result, the adaptation of these modulation index parameters makes the statistical verifications even more rigorous.

Throughout this paper, use is made of the VPI Photonics simulators and a simple IMDD network node, as illustrated in Fig. 1(a). In this Section, an input optical signal encoded using 10Gb/s 16-ary quadrature amplitude modulation (16-QAM) optical orthogonal frequency division multiplexing (OOFDM) is considered, which is generated by intensity-modulating a Mach-Zehnder modulator (IM-MZM). Immediately after the converter and prior to the square-law photon detection, the converted optical signal is injected into an ideal optical bandpass filter to select the converted optical component. Other adopted numerical simulation parameters that are not explicitly mentioned above are summarized in Table 1.

Table 1. Simulation Parameters

Item	Parameter	Value
DP-MZM	Insertion loss	7dB
	Extinction ratio	35dB
	Switching voltage V_π	5V
Optical signal	Central frequency	193.1THz
	Linewidth	10MHz
	Average power	6dBm
OFDM modulation	Cyclic prefix	12.5%
	Number of subcarriers	64
	Signal bit rate	$10 \sim 100$Gb/s
Driving RF signals	Frequency f_{RF}	30GHz
	Modulation index* $\beta_1, \beta_2, \beta_3, \beta_4$	1.84, 4.20, 6.42, 8.58,10.71

*Optimum β values used when the 1-, 3-, 5-, 7- and 9-*th* converted optical components are targeted.
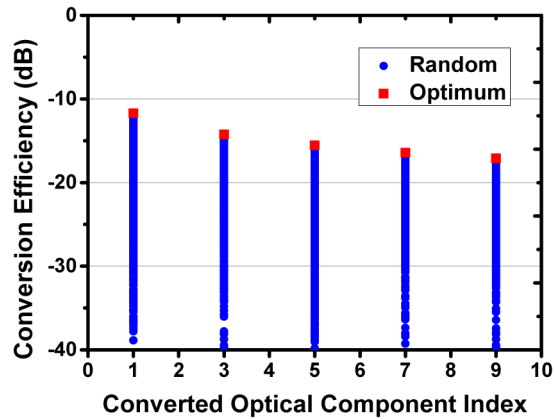
Fig. 3. Spectral conversion efficiencies of various converted optical components under optimum and randomly selected operating condition parameters.

Under the identified optimum operating conditions and the randomly selected operating condition parameters, the simulated spectral conversion efficiencies of various converted optical components are presented in Fig. 3, where 1600 randomly selected operating condition parameter sets are employed for each converted optical component targeted. It is very easy to see in Fig. 3 that the identified optimum operating conditions always offer the highest spectral conversion efficiencies, regardless of the converted optical component index.
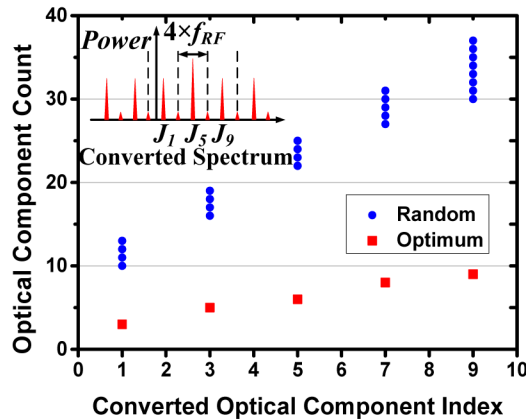
Fig. 4. Converted optical component index-dependent total number of parasitic optical components in the converted optical signals obtained under optimum and randomly selected operating condition parameters.

The impact of the identified optimum operating conditions on the minimization of the parasitic optical component count is shown in Fig. 4, where the total number of parasitic optical components is plotted for various converted optical components by utilizing the simulation parameters identical to those employed in Fig. 3. For the optimum operating conditions corresponding to the 5-*th* converted optical component, the converted optical signal spectrum is also inserted in Fig. 4. As analytically predicted in Section 2, Fig. 4 shows that the optimum operating conditions are capable of reducing the total number of parasitic optical components by approximately 75%. In addition, the dependence of the total number of parasitic optical components upon targeted optical component index is also significantly flattened, as seen in Fig. 4. In addition to the reduced cross-talk effect, the optimum operating condition-induced reduction in parasitic optical component count effectively increases the frequency spacing between two adjacent converted optical components from f_{RF} to $4 \times f_{RF}$

with f_{RF} being the driving RF signal frequency. This allows the utilization of a relatively low RF signal frequency to achieve a relatively large frequency detuning range with an enhanced spectral conversion efficiency.
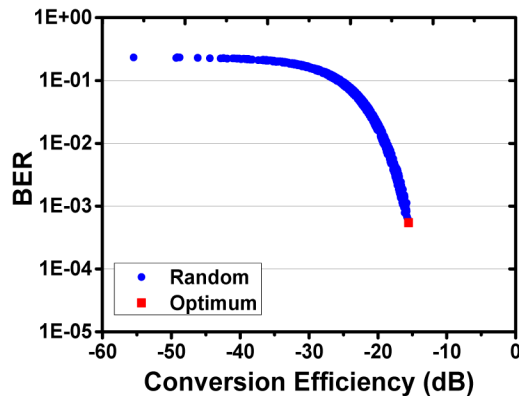

Fig. 5. BERs of the 5-*th* converted optical component for optimum and randomly selected operating condition parameters. The OSNR of input signal is fixed at 28dB.

In addition to the above-discussed spectral conversion efficiency maximization and the simultaneous parasitic optical component count minimization, the optimum operating conditions also result in the best BER performance of converted optical components, as presented in Fig. 5. In this figure, for both the optimum and 1600 randomly selected operating condition parameters, by making use of the simulation parameters similar to those in Fig. 3, the BER of the 5-*th* converted optical component is plotted as a function of spectral conversion efficiency for an input optical signal with a fixed OSNR of 28dB. It is very interesting to note in Fig. 5 that the optimum operating conditions offer not only the highest spectral conversion efficiency but also the lowest BER. In sharp contrast, when the optimum operating conditions are not satisfied, for the vast majority of cases where randomly selected operating conditions are employed, their corresponding BERs are well above the FEC limit of 1.0×10^{-3}.
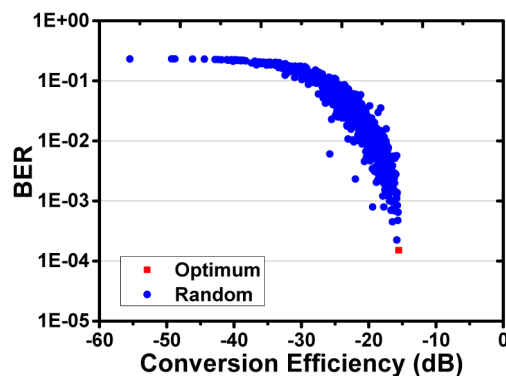

Fig. 6. BERs of the 5-*th* converted optical component for optimum and randomly selected operating condition parameters. The OSNR of the 5-*th* converted optical component is fixed at 20dB.

To further analysis the BER performance of the 5-*th* converted optical component for the cases similar to Fig. 5, Fig. 6 is plotted by taking into account the simulation parameters identical to those used in Fig. 5, except that the OSNR of the 5-*th* converted optical component is fixed at 20dB. In comparison with Fig. 5, a dispersed BER developing trend for

randomly selected operating conditions is observed, this is due to the fact that, to reach a specific BER, the 5-*th* converted optical component with a low OSNR allows a much wide range of converted optical component power variations.

4. Simulated spectral conversion performance

Having analytically identified and statistically verified the optimum operating conditions, the main objective of this section is to employ the optimum operating conditions to numerically explore achievable conversion performances of the proposed DP-MZM-based spectral converters in IMDD network nodes. The simulation parameters adopted in Section 3 and listed in Table 1 are still adopted here, unless explicitly stated in corresponding texts.

4.1 Frequency detuning range-dependent conversion efficiency

For the *p-th* converted optical component, its frequency detuning range, f_d, can be defined as

$$f_d = pf_{RF} \qquad (18)$$

where f_{RF} is the driving RF frequency. For f_{RF} = 30GHz, the trade-off between spectral conversion efficiency and frequency detuning range is shown in Fig. 7 for different input optical signal powers. As predicted by Eq. (16), due to the inherent property of the Bessel function of first kind, it can be seen in Fig. 7 that the spectral conversion efficiency decreases with increasing converted optical component index, p, and thus frequency detuning range. Moreover, such a developing trend is independent of input optical power.
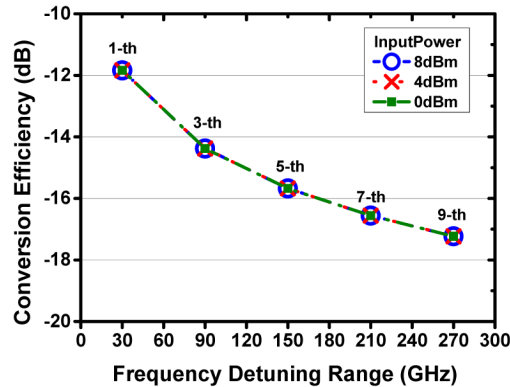

Fig. 7. Spectral conversion efficiency versus frequency detuning range for different input optical signal powers. The identified optimum operating conditions are adopted.

Here it is also worth mentioning the following two facts: i) Frequency detuning range-independent spectral conversion efficiency is also feasible when use is made of a variable driving RF frequency whilst the targeted optical component index remains constant; ii) For the *p-th* converted optical component, a reduction in DP-MZM insertion loss by *l*-dB gives rise to a *l*-dB enhancement in spectral conversion efficiency. Thus the DP-MZM insertion loss plays an important role in determining the practically achievable spectral conversion efficiency.

4.2 Spectral conversion-induced OSNR penalty

To investigate the impact of the proposed spectral converter on system OSNR penalty, for the 1-*st*, 5-*th* and 9-*th* converted optical components, their corresponding BER performances as a function of input signal OSNR are presented in Fig. 8(a), where the BER performance of a spectral conversion-free input optical signal is also plotted as a bench marker. It is shown in Fig. 8(a) that the spectral conversion-induced OSNR penalty at the FEC limit of 1.0×10^{-3} is approximately 4.8dB, 8.5dB and 9.8dB for the 1-*st*, 5-*th* and 9-*th* converted optical

components, respectively. Such observed OSNR penalty differences between different converted optical components are almost identical to their corresponding spectral conversion efficiency differences shown in Fig. 7. For example, for the 1-*st* and 5-*th* converted optical components, their OSNR penalty difference is 3.7dB, which is very similar to their spectral conversion efficiency difference of 3.8dB. This indicates that the resulting OSNR penalty originates mainly from the spectral conversion-associated reduction in optical power of the converted optical components.
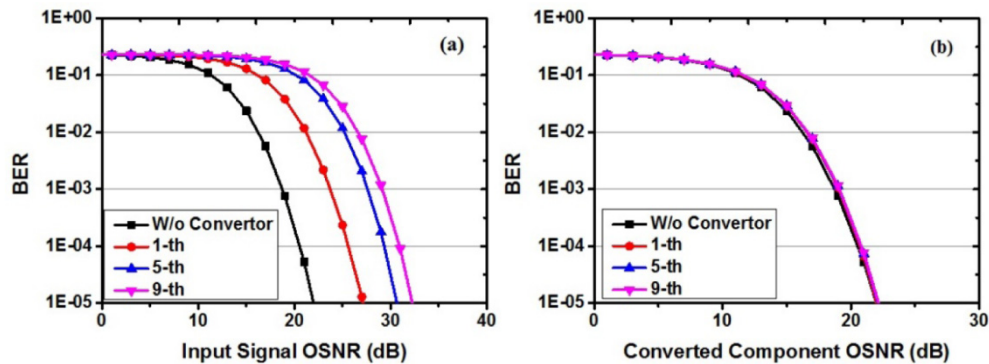
Fig. 8. BER versus signal OSNR for the 1-*st*, 5-*th* and 9-*th* converted optical components, as well as a spectral conversion-free input signal. (a) BER versus input signal OSNR; (b) BER versus converted component OSNR. The identified optimum operating conditions are adopted for all these two cases.

The above statement concerning the physical mechanism underpinning the spectral conversion-induced OSNR penalty is confirmed in Fig. 8(b), where the BER performances of the 1-*st*, 5-*th* and 9-*th* converted optical components are plotted against OSNR of the converted optical component. Figure 8(b) shows that all the BER curves of the converted optical components are perfectly overlapped with that corresponding to the conversion-free input optical signal. Apart from confirming the OSNR penalty's physical origin, such BER curve behaviors also imply that the proposed spectral conversion process is waveform-distortionless, regardless of the converted optical components targeted. This property is demonstrated in Fig. 9, where normalized signal waveform comparisons are made between the 1-*st*, 5-*th* and 9-*th* converted optical components and the conversion-free input optical signal. Perfect normalized waveform overlaps are observed in Fig. 9 between different converted optical components and the conversion-free input optical signal.
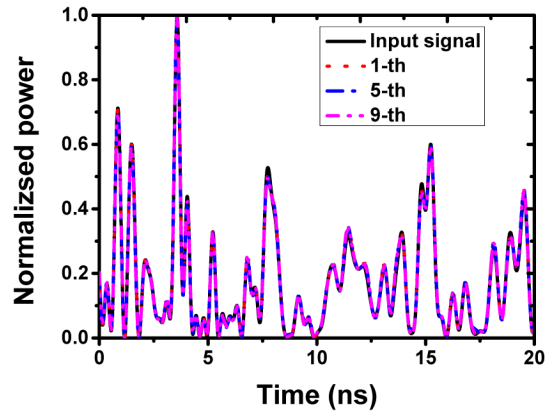
Fig. 9. Normalized signal waveforms of the 1-*st*, 5-*th* and 9-*th* converted optical components as well as the conversion-free input optical signal. The identified optimum operating conditions are adopted.

The above-mentioned unique spectral conversion features, namely distortionless waveforms in Fig. 9 and optical power reduction-induced OSNR penalties, indicate that the conversion operation of the proposed converter is linear. In practice, full use can be made of such a linear feature to realize the converter's reconfigurability, flexibility and elasticity without comprising its conversion performance. For instance, for OSNR-hungry traffic, use can be made of a low-order converted optical component to take full advantage of its high spectral conversion efficiency. This may require the driving RF signal to have a high frequency in order to align the converted optical component at a desired spectral region.

4.3 Transparency to input signal characteristics

As a direct result of the abovementioned linear spectral conversion operation, it is envisaged that the converter's performance is also strictly transparent to key system/network design factors including signal bit rate, signal spectral bandwidth and modulation format. To investigate the converter's performance transparency, Fig. 10 is presented, where use is made of various input optical signals with a wide diversity of properties, i.e. signal bit rates ranging from 10Gb/s to 100Gb/s, 10 times spectral bandwidth variations, and different signal modulation formats including QPSK and 16-QAM. In addition, the 5-*th* converted optical components are selected for all the cases considered.
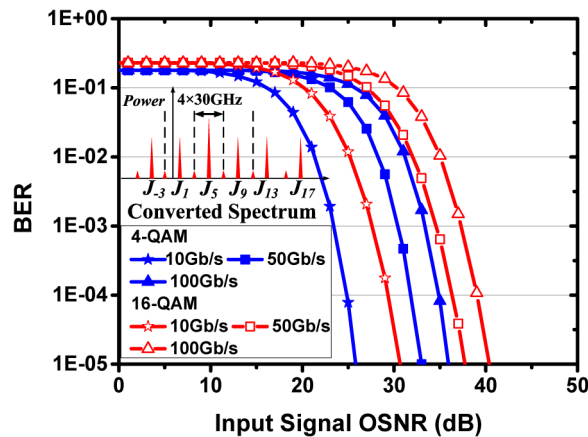

Fig. 10. 5-*th* converted optical component BER performances versus OSNR of input optical signals of various characteristics.

It is very interesting to note in Fig. 10 that almost parallel BER developing trends for BERs of $< 1.0 \times 10^{-2}$ are observed for all the considered cases. In particular, for the 4-QAM-encoded OOFDM signals, the differences in the minimum required OSNR at a BER of 1.0×10^{-3} between different signal bit rates are almost identical to those corresponding to the 16-QAM-encoded OOFDM signals of the same signal bit rates. For example, the observed OSNR differences between 10Gb/s and 50Gb/s are approximately 7.7dB for both the 4-QAM- and 16-QAM-encoded OOFDM signals. This indicates that the spectral conversion operation of the proposed converter has excellent performance transparency to signal modulation format, signal spectral bandwidth and signal bit rate.

To avoid the cross-talk effect between two adjacent converted optical components, the maximum allowable signal spectral bandwidth is determined by the spectral difference between two adjacent converted optical components, i.e. $4 \times f_{RF} = 120$GHz for the considered cases. Our simulations show that the cross-talk effect is negligible when the signal spectral bandwidths are smaller than $3.3 \times f_{RF}$.

4.4 Impact of optical filter width on spectral conversion performance

In all numerical simulations discussed previously, use is made of ideal optical filters with $4 \times f_{RF}$ bandwidths and their central frequencies located at the converted optical components. Given the fact that the properties of different converted optical components are strongly related to each other, it is, therefore, expected that the requirement on narrow optical filters can be relaxed significantly.

To explore the impact of optical filter bandwidth on the converter performance, for 10Gb/s 16-QAM-encoded OOFDM input signals, the corresponding BER performances of the 5-*th* converted optical components as a function of input signal OSNR are presented in Fig. 11, by making use of various optical filters having bandwidths of 120GHz, 240GHz and 360GHz. For the considered converter parameters, such adopted filter bandwidths allow one, two and three converted optical components to simultaneously reach the square-law photon detector. For comparisons, an extreme case without using any optical filters is also given in Fig. 11.

It is shown in Fig. 11 that very similar BER performances occur for all these different optical filters, implying that the impact of optical filter bandwidth on the converter performance is negligible. For the case without including any optical filters, the BER performance is, however, slightly improved in comparison with the cases of utilizing narrow bandwidth optical filters. This is because the presence of multiple converted optical components with dedicated phase relationships enhances the detected baseband signal power and thus its OSNR. The observed optical filter bandwidth relaxation can greatly simplify the converter configuration architecture, reduce its footprint and power consumptions, as well as lower its cost.
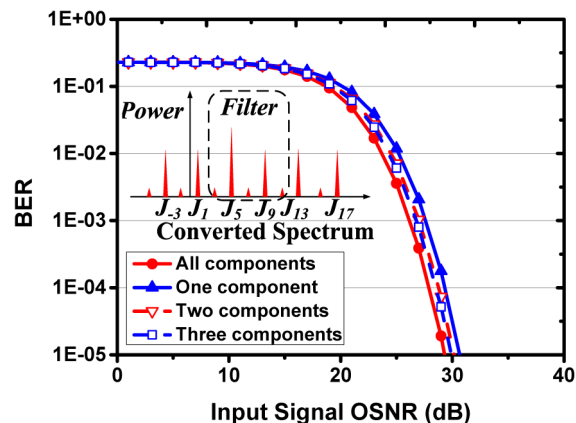
Fig. 11. 5-*th* converted optical component BER performances versus OSNR of input signal for different widths of optical filters.

4.5 Impact of DP-MZM extinction ratio on spectral conversion performance

To demonstrate the impact of the DP-MZM extinction ratio on the spectral conversion performance, for the 1-, 5- and 9-*th* converted optical components, their corresponding conversion efficiencies, the number of parasitic optical components and their BER performances are plotted in Figs. 12(a)-12(c), respectively, as a function of DP-MZM extinction ratio. In obtaining Fig. 12, the OSNR of each converted optical component is fixed at 20dB. From Fig. 12(a), it is easy to see that the conversion efficiency is independent of extinction ratio, regardless of the chosen converted optical component. As shown in Fig. 12(b), when the 1-*st* optical component is chosen to be the converted one, its corresponding parasitic component count can reach a minimization similar to that in Fig. 4, for extinction ratios as low as 20dB. Whilst when the 5-*th* and 9-*th* optical components are chosen as the converted ones, their corresponding parasitic component count still reach their minimum for extinction ratios of >35dB. As a direct result of the extinction ratio-independent conversion efficiency presented in Fig. 12(a), for the fixed 20dB OSNRs of different converted optical components, flat BER curves are thus observed in Fig. 12(c). It can be seen in Fig. 12(c) that for 10Gb/s 16-QAM-encoded OOFDM input signals, the 1-, 5- and 9-*th* converted optical components give rise to almost identical BER performances, which are again independent of extinction ratio.
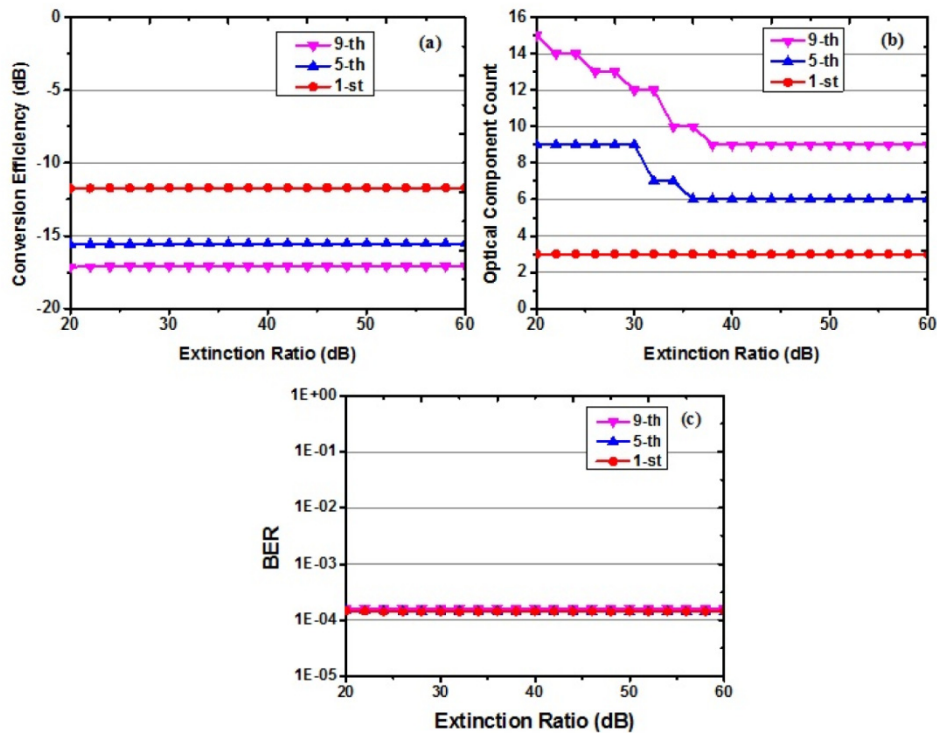
Fig. 12. Impacts of DP-MZM extinction ratio on the spectral converter performance for the 1-, 5- and 9-*th* converted optical components. (a) conversion efficiency versus extinction ratio, (b) total number of parasitic optical components versus extinction ratio, and (c) BER performance versus extinction ratio. In calculating these three figures, the OSNR of each converted optical component is fixed at 20dB.

From the above discussions, it can be seen that: a) for practical DP-MZMs, the impact of their infinite extinction ratio on the converter performance can be negligible, b) DP-MZMs with relatively high ERs ensure a better suppression of unwanted parasitic components, c) the low-order converted optical component has improved robustness to extinction ratio variations compared to high-order converted optical components.

5. Experimentally measured spectral conversion performance

To verify the theoretical predictions presented in Section 3 and Section 4, in this section, experimental investigations of the spectral conversion performance of the proposed converter under various operating conditions are undertaken utilizing the experimental setup illustrated in Fig. 1(a).

As seen in Fig. 1(a), a CW optical light source with a wavelength of 1550.118 nm and a 13dBm output optical power is firstly intensity-modulated by a MZM subject to an arbitrary waveform generator-produced 10Gb/s 16-QAM OFDM signal. After passing through an EDFA and a variable optical attenuator, the modulated optical signal is then injected into an integrated 12.5dB insertion loss and 22dB ER DP-MZM (Fujitsu 7967EQA) to perform the spectral conversion.

An electrically amplified 12.5GHz sinusoidal RF signal is employed as a driving RF signal, which is split into four driving RF signals by a phase shifter. Each driving RF signal is injected into one of the four DP-MZM electrodes. To satisfy the identified optimum operating conditions, the amplitudes of these four driving RF signals are always kept identical and finely adjusted according to the order of the converted optical component. In addition, their corresponding phases are shifted to 0, 90, 180 and 270 degrees, respectively. The DP-MZM-

converted optical signal passes through an optical tunable filter to select the converted optical component. The filtered optical component is then detected by a 12GHz photodetector, and the detected electrical signal is captured by a digital storage oscilloscope and finally processed offline.

For an input 10Gb/s OOFDM signal of 7.9dBm, Fig. 13(a) shows a representative converted optical spectrum immediately after the DP-MZM subject to the optimum operating conditions for the 1-*st* converted optical component. For comparison, a corresponding optical spectrum without satisfying the optimum operating conditions is also presented in Fig. 13 (b), in obtaining Fig. 13(b), the DC bias currents are randomly shifted from their corresponding optimum values. By comparing the aforementioned two figures, it can be easily seen that the adaptation of the optimum operating conditions for the 1-*st* converted optical component significantly enhances the optical power of the 1-*st* converted optical component only, and simultaneously gives rise to >35dB optical power reduction for all the even-order optical components and half of the odd-order optical components. This confirms that the optimum operation conditions can reduce 75% of the parasitic optical components. In addition, based on Fig. 13(a), the spectral conversion efficiency of the 1-*st* converted optical component can also be calculated as −9.5dBm - 7.9dBm = −17.4dB, which agrees very well with Eq. (16) when the DP-MZM insertion loss of 12.5dB is considered.
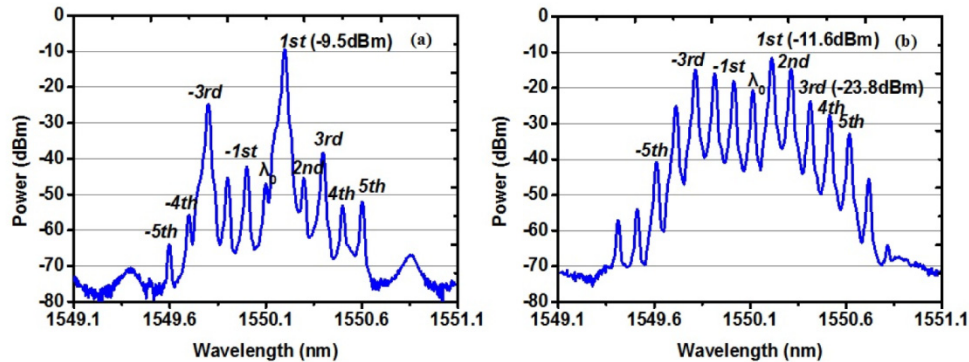

Fig. 13. Representative optical spectrum (a) emerging from the DP-MZM subject to the optimum operating conditions for the 1-*st* converted optical component; (b) emerging from the DP-MZM subject to non-optimized operating conditions.

Furthermore, when the DP-MZM operating conditions are set to be optimum for the 3-rd converted optical component, the corresponding spectral conversion performances very similar to those presented in Fig. 13(a) are still obtainable, except that the following three major differences occur: i) as expected, the 3-rd converted optical component has the highest optical power of −12.3dBm; ii) the corresponding conversion efficiency is −12.3dBm - 7.9dBm = −20.2dB, which is just ~0.4dB lower than that predicated by Eq. (16); and iii) compared to the 1-st converted optical component case, the parasitic optical component powers increase because of the imperfect DP-MZM-caused slight imbalance between two optical signals associated with MZ-a and MZ-b, as shown in Fig. 1(a). As predicted in numerical simulations, the impact of the imbalance effect on the parasitic optical component power increases with increasing the order of the converted optical component.

Here it is also worth pointing out that the experimentally measured conversion efficiency difference between the 1-st and 3-rd converted optical components is very close to that predicated by Eq. (16). This implies that the frequency detuning range-independent conversion efficiency is feasible when use is made of variable driving RF frequency with the targeted order of the converted optical component remaining the same.
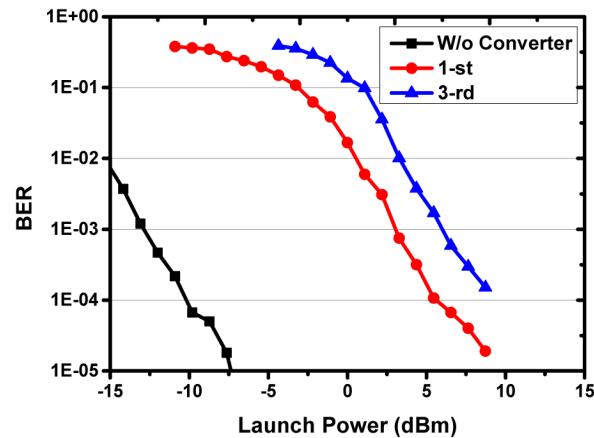
Fig. 14. BERs versus optical launch power for the 1-*st* and 3-*rd* converted optical components each obtained under its optimum operating conditions. A BER curve for the spectral conversion-free input optical signal is also plotted for comparison.
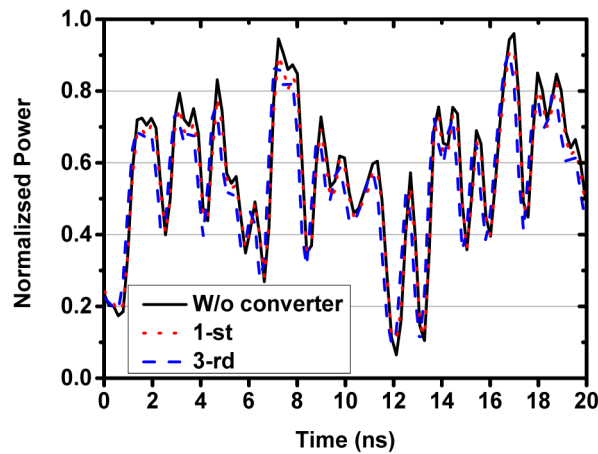

Fig. 15. Normalized signal waveforms of the 1-*st* and 3-*rd* converted optical component as well as the conversion-free input optical signal. In measuring the waveforms of the converted optical components, the identified optimum operating conditions are adopted.

For different converted optical components each obtained under its optimum operating conditions, the proposed converter-induced power penalties are examined in Fig. 14, where corresponding BERs as a function of optical launch power are plotted, where the DP-MZM insertion loss effect is taken into acount. It is shown in Fig. 14 that the spectral conversion-induced power penalty at the FEC limit of 1.0×10^{-3} is approximately 16.2dB and 19.1dB for the 1-st and 3-rd converted optical components, respectively. Between these two components, there exists a power penalty difference of 2.9dB, which is almost identical to their corresponding spectral conversion efficiency difference of 2.8dB, as discussed above. This indicates that the resulting power penalty mainly originates from the reduced conversion efficiency.

The theoretically predicted linear spectral conversion process is experimentally confirmed in Fig. 15, where normalized signal waveform comparisons are made between the 1-st and 3-rd converted optical components as well as the conversion-free input optical signal. Very similar to the numerically simulated results in Fig. 9, these three measured waveforms are almost identical, indicating that the spectral conversion operation is linear and waveform-distortionless.

6. Conclusions

A simple DSP-enabled reconfigurable and transparent signal spectral converter has been proposed and extensively investigated, for the first time, by just utilizing a single standard DP-MZM driven by SDN controllable RF signals and DC bias currents. Optimum operating conditions of the proposed converter have been analytically identified, statistically examined and experimentally verified, based on which spectral conversion performances in IMDD-based network nodes are extensively explored both theoretically and experimentally in terms of frequency detuning range-dependent conversion efficiency, spectral conversion-induced OSNR/power penalty, transparency to input signal characteristics, as well as opportunity for further simplifying the proposed converter architecture. Our results have shown that the proposed converter has unique advantages including, for example, low configuration complexity, strict transparency, SDN-controllable reconfigurability and flexibility, as well as negligible spectral conversion-induced latency. This work suggests that the proposed spectral converter is promising for seamlessly integrating traditional metropolitan optical networks and future mobile backhaul networks.